

**OPTICAL METROLOGY BY CIRCULAR
GRATING TALBOT INTERFEROMETER AND
DIGITAL HOLOGRAPHY**

SHILPI AGARWAL



INSTRUMENT DESIGN DEVELOPMENT CENTRE

INDIAN INSTITUTE OF TECHNOLOGY DELHI

NEW DELHI – 110016, INDIA

JULY 2018

© Indian Institute of Technology Delhi (IITD), New Delhi, 2018

**OPTICAL METROLOGY BY CIRCULAR
GRATING TALBOT INTERFEROMETER AND
DIGITAL HOLOGRAPHY**

by

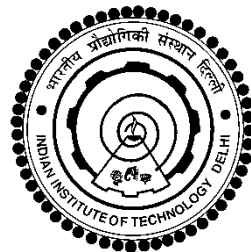
SHILPI AGARWAL

INSTRUMENT DESIGN DEVELOPMENT CENTRE

Submitted

in fulfillment of the requirements of the degree of Doctor of Philosophy

to the



INDIAN INSTITUTE OF TECHNOLOGY DELHI

JULY 2018

DEDICATED
TO
TWO MEN IN MY LIFE

(Success is in my side, because I have you two by my side)

*My father - for his endless love, support and
encouragement*

*My Husband - for being my inspiration, his remarkable
patience and unwavering love who dragged me even through
kicking most of the way*

CERTIFICATE

This is to certify that the thesis entitled, “**OPTICAL METROLOGY BY CIRCULAR GRATING TALBOT INTERFEROMETER AND DIGITAL HOLOGRAPHY**” being submitted by **Ms. SHILPI AGARWAL**, to the Indian Institute of Technology Delhi, for the award of the degree of “**DOCTOR OF PHILOSOPHY**” is a record of the bonafide research work carried out by her under my supervision and guidance. She has fulfilled all the requirements for submission of this thesis, which to the best of my knowledge has reached the required standard.

The material contained in this thesis has not been submitted in part or full to any other University or Institute for the award of any other degree.

Dr. Chandra Shakher
Emeritus Professor
Instrument Design Development Centre
Indian Institute of Technology Delhi
Hauz Khas-110016, New Delhi, India

ACKNOWLEDGEMENTS

First and foremost, I would like to express my special appreciation and thanks to my supervisor **Professor Chandra Shakher**, for being a tremendous mentor for me. Credit of introducing me to the area of Optical Metrology goes solely to him. I would like to thank him for encouraging my research and for allowing me to grow as a research scientist. His patience, motivation, enthusiasm, immense knowledge and advice on both research, as well as on my career have been priceless. Prof. Chandra Shakher has on several occasions, put in hours of hard work to sort out intractable problems. Without his excellent insight into the topic and for his continuous guidance, the work being reported upon in this thesis would not have been completed. I have been extremely lucky to have a supervisor who cared so much about my work, and who responded to my questions and queries so promptly. His guidance helped me in all the time of research and writing of this thesis. Apart from the subject of my research, I learnt a lot from him, which I am sure will be useful in different stages of my life. I solemnly submit my honest and humble thanks to him for bringing my dreams into reality. I could not have imagined having a better supervisor and mentor for my Ph.D. study.

I am grateful to all my student research committee (SRC) members, **Prof. M. R. Shenoy**, **Prof. A. L. Vyas**, **Prof. D. S. Mehta** and **Dr. Gufran S. Khan** for providing technical advice, constant encouragement, insightful comments and inspiration. It is my duty to record sense of gratitude to **Dr. Satish Dubey** for his encouragement and the entire faculty of Instrument Design Development Centre.

The days would have passed far more slowly without the support of my best friend, **Dr. Manoj Kumar**, whom I thank for tolerating my idiosyncrasies and crazy habits and for

providing such a rich source of conversation, education and entertainment. It is with immense pleasure I express my thankfulness to my friend and colleague, **Dr. Varun Kumar** for always been there with a helping hand throughout the period of my research work. I would also like to thank him for his help, co-operation and hustle during the tenure of my work. I sincerely acknowledge my senior colleagues **Dr. Gyanendra Sheoran** and **Dr. Shobhna Sharma** for their support and encouragement in my research work. I also extend my thanks fellow lab mates **Mr. Vivek Rastogi, Ms. Ritambhara, Ms. Sruthi Prasood, Ms. Monika, Mr. Avijit Prakash Singh** and **Mr. Pranav Kumar Pandey** for all the support, motivation and all the fun we have had in the last few years.

Thanks are also due to the technical staff of the workshop in instrument design development centre for the help rendered by them.

Everything would be incomplete without mentioning my family. I must express my gratitude to **Kunal**, my husband, for his moral support and encouragement. Thank you for teaching me that my job in life was to learn, to be happy, and to know and understand myself; only then could I know and understand others. Thank you to my father, **Subhash Agarwal**, for believed in me, encouraging me in all of my pursuits and inspiring me to follow my dreams, my mother, **Sarita Agarwal**, for guiding me as a person and wanted the best for me. Words cannot express how grateful I am to my mother-in law **Sudesh Gupta** and father-in-law **R. K. Gupta** for all of the sacrifices that they've made on my behalf.

It's my fortune to gratefully acknowledge the support of my younger sister **Chetna Agarwal** and brother **Shobhit Agarwal**. They were always beside me during the happy and hard moments to push me and motivate me. My sister was always there for me in my failures,

weird situations and tolerated my frustrations, irritations and nonsenses without complaining. Your prayer for me was what sustained me thus far. Finally, I would like to thank God, the Almighty for his immeasurable help at every stage of my work. There is no way to express how much it meant to me to have been a member of **Laser Applications and Holography Laboratory**.

Date:

Shilpi Agarwal

ABSTRACT

Optics relates to the generation, amplification, propagation, reception, modification and modulation of light. In brief, *Optics* is science, technology and engineering with light. Measurement techniques based on properties of light come under *Optical Metrology*. Optical interferometric techniques provide improved accuracy/precision over mechanical methods of measurement; such techniques provide non-destructive testing (NDT), have higher resolution and dynamic range and allow the recognition of flaws and defects in materials and components. At present many optical interferometric measurement and non-destructive testing techniques, like classical interferometry, shearing interferometry, Moiré interferometry, fringe projection technique, Lau phase interferometry, holographic interferometry, speckle pattern interferometry and Talbot interferometry etc. are available. Optical interferometric techniques for measurement and NDT are sensitive to environmental perturbations, while from the industrial perspective one need a method which is accurate, cost-effective and capable to work in industrial environment.

Talbot interferometer has been used for the measurement of displacement, collimation, focal length, refractive index, low frequency vibrations and temperature etc. In this thesis, three new applications of circular grating Talbot interferometer are investigated. Further, digital holographic interferometry is investigated for measurement of temperature and temperature profile of micro flame under the influence of magnetic field.

The thesis is organized in six chapters:

Chapter I provide a brief introduction of Talbot interferometer and the detailed description of linear grating and circular grating Talbot interferometer under plane wave and spherical wave

illumination. This chapter also provides the outline of the research work presented in this thesis.

Chapter II presents the investigations of in-plane displacement measurement by using circular grating Talbot interferometer. The measurement of shift of fringe position from the grating center is used to measure the in-plane displacement. This method can be used as an alternative method of measurement of in-plane displacement.

Chapter III gives the experimental investigations of the effect of magnetic field on temperature and temperature profile of butane diffusion flame, premixed flame and partially premixed flame (with 50% air) using circular grating Talbot interferometer. This investigation is useful to improve the combustion process and increase the combustion efficiency.

Chapter IV presents the measurement of the temperature and temperature profile of wick-stabilized micro-diffusion flame under the influence of magnetic field using circular grating Talbot interferometer. In this chapter the phase information is extracted by Hilbert transform to obtain the full field data from a single interferogram.

Chapter V deals with a method for measurement of temperature and temperature fluctuations in wick-stabilized micro diffusion flame using digital holographic interferometry. Digital holography is ideally suited to study micro flames.

Chapter VI described the Talbot effect/self-imaging effect for cell level imaging of biological specimens (Onion epidermis cell, Red blood cell) using linear grating. Experimental results show that this type of system can be used for clinical applications.

सार

प्रकाशिकी पीढ़ी, प्रवर्धन, प्रसार, स्वागत, संशोधन और प्रकाश के माँड्यूलेशन से संबंधित है। संक्षेप में, प्रकाशिकी विज्ञान के साथ विज्ञान, प्रौद्योगिकी और इंजीनियरिंग है। प्रकाश की गुणों के आधार पर मापन तकनीक ऑप्टिकल मेट्रोलॉजी के अंतर्गत आती है। ऑप्टिकल इंटरफेरोमेट्रिक तकनीक माप के यांत्रिक तरीकों पर बेहतर सटीकता / सटीकता प्रदान करती है; ऐसी तकनीकें गैर-विनाशकारी परीक्षण (एनडीटी) प्रदान करती हैं, उच्च रिज़ॉल्यूशन और गतिशील रेंज होती है और सामग्री और घटकों में त्रुटियों और दोषों की पहचान की अनुमति देती है। वर्तमान में कई ऑप्टिकल इंटरफेरोमेट्रिक मापन और गैर-विनाशकारी परीक्षण तकनीकों, जैसे शास्त्रीय इंटरफेरोमेट्री, कतरन इंटरफेरोमेट्री, मोइरे इंटरफेरोमेट्री, फ्रिंज प्रक्षेपण तकनीक, लॉउ चरण इंटरफेरोमेट्री, होलोग्राफिक इंटरफेरोमेट्री, स्कलेल पैटर्न इंटरफेरोमेट्री और टैलबोट इंटरफेरोमेट्री आदि उपलब्ध हैं। माप और एनडीटी के लिए ऑप्टिकल इंटरफेरोमेट्रिक तकनीक पर्यावरण संबंधी परेशानियों के प्रति संवेदनशील हैं, जबकि औद्योगिक परिप्रेक्ष्य से किसी को एक ऐसी विधि की आवश्यकता होती है जो सटीक, लागत प्रभावी और औद्योगिक वातावरण में काम करने में सक्षम हो।

टैलबोट इंटरफेरोमीटर का उपयोग विस्थापन, कोलाइमन, फोकल लम्बाई, अपवर्तक सूचकांक, कम आवृत्ति कंपन और तापमान इत्यादि के माप के लिए किया गया है। इस थीसिस में, सर्कुलर ग्रेटिंग टैलबोट इंटरफेरोमीटर के तीन नए अनुप्रयोगों की जांच की जाती है। इसके अलावा, चुंबकीय क्षेत्र के प्रभाव में सूक्ष्म लों के तापमान और तापमान प्रोफाइल के माप के लिए डिजिटल होलोग्राफिक इंटरफेरोमेट्री की जांच की जाती है।

थीसिस छह अध्यायों में आयोजित किया जाता है:

अध्याय I में टैलबोट इंटरफेरोमीटर का एक संक्षिप्त परिचय प्रदान करता हूँ और रैखिक ग्रेटिंग और सर्कुलर ग्रेटिंग टैलबोट इंटरफेरोमीटर का विस्तृत विवरण विमान लहर और गोलाकार लहर रोशनी के तहत प्रदान करता हूँ। यह अध्याय इस थीसिस में प्रस्तुत शोध कार्य की रूपरेखा भी प्रदान करता है।

अध्याय II सर्कुलर ग्रेटिंग टैलबोट इंटरफेरोमीटर का उपयोग करके इन-प्लेन विस्थापन माप की जांच प्रस्तुत करता है। ग्राउटिंग सेंटर से फ्रिंग स्थिति की शिफ्ट का माप इन-प्लेन विस्थापन को मापने के लिए किया जाता है। इस विधि को इन-प्लेन विस्थापन के माप के वैकल्पिक तरीके के रूप में उपयोग किया जा सकता है।

अध्याय III परिपत्र ग्राउटिंग टैलबोट इंटरफेरोमीटर का उपयोग करके ब्यूटेन प्रसार आग, प्रीमिस्ड लौ और आंशिक रूप से प्रीमिस्ड लौ (50% हवा के साथ) के तापमान और तापमान प्रोफाइल पर चुंबकीय क्षेत्र के प्रभाव की प्रयोगात्मक जांच देता है। यह जांच दहन प्रक्रिया में सुधार और दहन दक्षता में वृद्धि के लिए उपयोगी है।

अध्याय IV परिपत्र ग्राउटिंग टैलबोट इंटरफेरोमीटर का उपयोग करके चुंबकीय क्षेत्र के प्रभाव में विक-स्थिरीकृत माइक्रो-प्रसार फ़्यूम के तापमान और तापमान प्रोफाइल के माप को प्रस्तुत करता है। इस अध्याय में चरण जानकारी हिल्बर्ट ट्रांसफॉर्म द्वारा एक इंटरफेरोग्राम से पूर्ण फ़ील्ड डेटा प्राप्त करने के लिए निकाला जाता है।

अध्याय V डिजिटल होलोग्रफिक इंटरफेरोमेट्री का उपयोग करते हुए विक-स्थिरीकृत माइक्रो प्रसार फ़्लेम में तापमान और तापमान में उतार-चढ़ाव के माप के लिए एक विधि से संबंधित है। डिजिटल होलोग्राफी आदर्श रूप से सूक्ष्म आग का अध्ययन करने के लिए उपयुक्त है।

अध्याय VI ने रैखिक समानांतर तारों का समूह का उपयोग कर जैविक नमूने (प्याज एपिडर्मिस सेल, लाल रक्त कोशिका) के सेल स्तर इमेजिंग के लिए टैलबोट प्रभाव / स्वयं इमेजिंग प्रभाव का वर्णन किया। प्रायोगिक परिणामों से पता चलता है कि इस प्रकार की प्रणाली का उपयोग नैदानिक अनुप्रयोगों के लिए किया जा सकता है।

CONTENTS

<i>CERTIFICATE</i>	i
<i>ACKNOWLEDGEMENTS</i>	ii
<i>ABSTRACT</i>	v
<i>CONTENTS</i>	ix
<i>LIST OF FIGURES</i>	xiv
<i>LIST OF TABLES</i>	xxvi
<i>LIST OF SYMBOLS</i>	xxvii
CHAPTER 1: Talbot Interferometer: from Principle to Applications	1-31
1.1 Introduction	
1.2 Talbot effect	
1.3 Talbot interferometer	
1.3.1 Linear grating Talbot interferometer	
1.3.1.1 Collimated illumination (Plane wave)	
1.3.1.2 De-collimated illumination (spherical wave)	
1.3.2 Circular grating Talbot interferometer	
1.3.2.1 Collimated illumination (Plane wave)	
1.3.2.2 De-collimated illumination (spherical wave)	
1.4 Effect of source coherence, grating size, dimensions and grating orientation on self-imaging	

- 1.4.1 Effect of source coherence
- 1.4.2 Effect of grating dimension/periodicity error
- 1.4.3 Effect of grating orientation
- 1.5 Sensitivity and Contrast
- 1.6 Applications of Talbot interferometry
- 1.7 Outlines of the research work done in the thesis

CHAPTER 2: In-Plane Displacement Measurement by using Circular Grating Talbot Interferometer 32-54

- 2.1 Introduction
- 2.2 Theory
- 2.3 Experimental
 - 2.3.1 Set-up
 - 2.3.2 Measurement procedure and analysis
- 2.4 Results and Discussions
- 2.5 Conclusion

CHAPTER 3: Experimental Investigation of the Effect of Magnetic Field on Temperature and Temperature Profile of Gaseous Flame using Circular Grating Talbot Interferometer 55-82

- 3.1 Introduction
- 3.2 Theory
- 3.3 Experimental
- 3.4 Results
 - 3.4.1 Diffusion flame

- 3.4.2 Partially premixed (butane +50% air (oxidizer)) flame
- 3.4.3 Premixed flame
- 3.5 Discussion
- 3.6 Conclusion

CHAPTER 4: Measurement of Temperature and Temperature Profile of Wick-Stabilized Micro-Diffusion Flame under the Influence of Magnetic field using Circular Grating Talbot Interferometer 83-106

- 4.1 Introduction
- 4.2 Difference between macro (cm. size) and micro (mm. size) flame
- 4.3 Micro flames
- 4.4 Self-trimming of candle wick for the creation of micro-diffusion flame
- 4.5 Theory
 - 4.5.1 Phase Extraction by using Hilbert Transform
 - 4.5.2 Refractive index and Temperature Measurement
- 4.6 Experimental
- 4.7 Results
- 4.8 Discussion
- 4.9 Conclusion

CHAPTER 5: Measurement of Temperature and Temperature Profile of Wick Stabilized Micro Diffusion Flame under the Influence of Magnetic Field Using Digital Holographic Interferometry (DHI) 107-137

5.1	Introduction	
5.2	Digital holography	
5.2.1	Recording of digital holograms	
5.2.2	Numerical reconstruction of digital holograms	
5.2.3	Lensless Fourier Transform Digital Holography	
5.3	Experimental	
5.4	Results	
5.4.1	Temperature measurement of micro flame in the case of uniform, upward decreasing and upward increasing magnetic field	
5.4.2	Flame stability	
5.4.3	Comparison of normal diffusion flame and micro diffusion flame	
5.5	Discussion	
5.6	Conclusion	

CHAPTER 6: Cell imaging by using Talbot Effect	138-160
-------------------------------------------------------	---------

6.1	Introduction	
6.2	Theory	
6.3	Experiment set up-1 (Onion cell imaging)	
6.4	Experiment set up-2 (Red Blood cell imaging)	
6.5	Results	
6.6	Conclusion	

CHAPTER 7: Conclusion	161
------------------------------	-----

<i>FUTURE SCOPE OF THE WORK</i>	162
----------------------------------------	-----

<i>REFERENCES</i>	163-190
<i>ANNEXURES</i>	191-198
Annexure-I: Phase extraction by Hilbert transform method	
Annexure-II: Phase shifting method	
Annexure-III: Convolution method	
Annexure-IV: Angular spectrum method	
<i>LIST OF PUBLICATIONS</i>	199-200
<i>AUTHOR'S BIOGRAPHY</i>	201

LIST OF FIGURES

Fig. 1.1	Schematic of Talbot effect
Fig. 1.2	Experimental Talbot carpet of light
Fig. 1.3	Schematic of linear grating Talbot interferometer for plane wave illumination
Fig. 1.4	Schematic of linear grating Talbot interferometer for spherical wave illumination
Fig. 1.5	Schematic of circular grating representing Eq. (1.25)
Fig. 1.6	Schematic of circular grating Talbot interferometer
Fig. 1.7(a)	Schematic of circular grating Talbot interferometer for de-collimated illumination Medieval view
Fig. 1.7(b)	Schematic of circular grating Talbot interferometer for de-collimated illumination 3D view
Fig. 1.8	Walk-off effect geometry
Fig. 1.9	Plot of sensitivity variation in term of deflection angle with Talbot plane (Theoretical)
Fig. 2.1	Displacement between two gratings
Fig. 2.2	Simulated intensity distribution for zeroth order fringe
Fig. 2.3	Simulated intensity distribution for first order fringe
Fig. 2.4	Simulated intensity distribution for second order fringe

Fig. 2.5	Schematic of experimental set-up of Talbot interferometer
Fig. 2.6	Photograph of experimental set-up of Talbot interferometer
Fig. 2.7	Recorded interferogram for two displaced grating (5 μm to 1000 μm)
Fig. 2.8	Measurement algorithm for in-plane displacement
Fig. 2.9(a)	Recorded interferogram
Fig. 2.9(b)	Background normalization
Fig. 2.9(c)	Dilated interferogram for grating removal
Fig. 2.10(a)	Dilated Talbot interferometric fringe pattern for no displacement
Fig. 2.10(b)	Dilated Talbot interferometric fringe pattern for displacement 50 μm
Fig. 2.11(a)	Intensity distribution along grating center for no displacement
Fig. 2.11(b)	Intensity distribution along grating center for displacement 50 μm
Fig. 2.12	Intensity distribution along grating center for zeroth order fringe (10 μm , 20 μm , 30 μm)
Fig. 2.13(a)	Measured displacement vs. given displacement for zeroth order at sixth Talbot plane
Fig. 2.13(b)	Measured displacement vs. given displacement for first order at sixth Talbot plane
Fig. 2.13(c)	Measured displacement vs. given displacement for second order at sixth Talbot plane

Fig. 2.14(a)	Difference in measurement by micrometer and Talbot interferometry for displacement range 5-50 μm
Fig. 2.14(b)	Difference in measurement by micrometer and Talbot interferometry for displacement range 50-350 μm
Fig. 2.14(c)	Difference in measurement by micrometer and Talbot interferometry for displacement range 350-1000 μm
Fig. 3.1(a)	Schematic of experimental set-up of Talbot interferometer for temperature measurement
Fig. 3.1(b)	Photograph of experimental set-up of Talbot interferometer for temperature measurement
Fig. 3.2	Schematic representation of different position of flame in magnetic field
Fig. 3.3(a)	Photograph and recorded interferogram of diffusion flame of butane torch burner in absence of magnetic field
Fig. 3.3(b)	Photograph and recorded interferogram of diffusion flame of butane torch burner in uniform magnetic field
Fig. 3.3(c)	Photograph and recorded interferogram of diffusion flame of butane torch burner in upward-decreasing magnetic field
Fig. 3.3(d)	Photograph and recorded interferogram of diffusion flame of butane torch burner in upward-increasing magnetic field
Fig. 3.4(a)	Refractive index difference of diffusion flame of butane torch burner in the absence of magnetic field
Fig. 3.4(b)	Temperature distribution of diffusion flame of butane torch burner in the absence of magnetic field

Fig. 3.4 (c)	Comparison of experimental data with thermocouple data of temperature distribution of diffusion flame in the absence of magnetic field
Fig. 3.5(a)	Refractive index difference of diffusion flame of butane torch burner in the uniform magnetic field
Fig. 3.5(b)	Temperature distribution of diffusion flame of butane torch burner in the uniform magnetic field
Fig. 3.6(a)	Refractive index difference of diffusion flame of butane torch burner in the upward-decreasing magnetic field
Fig. 3.6(b)	Temperature distribution of diffusion flame of butane torch burner in the upward-decreasing magnetic field
Fig. 3.7(a)	Refractive index difference of diffusion flame of butane torch burner in the upward-increasing magnetic field
Fig. 3.7(b)	Temperature distribution of diffusion flame of butane torch burner in the upward-increasing magnetic field
Fig. 3.8(a)	Photograph and recorded interferogram of partially premixed flame of butane torch burner in absence of magnetic field
Fig. 3.8(b)	Photograph and recorded interferogram of partially premixed flame of butane torch burner in uniform magnetic field
Fig. 3.8(c)	Photograph and recorded interferogram of partially premixed flame of butane torch burner in upward-decreasing magnetic field
Fig. 3.8(d)	Photograph and recorded interferogram of partially premixed flame of butane torch burner in upward-increasing magnetic field
Fig. 3.9(a)	Refractive index difference of partially premixed flame of butane torch burner in the absence of magnetic field

Fig. 3.9(b)	Temperature distribution of partially premixed flame of butane torch burner in the absence of magnetic field
Fig. 3.10(a)	Refractive index difference of partially premixed flame of butane torch burner in the uniform magnetic field
Fig. 3.10(b)	Temperature distribution of partially premixed flame of butane torch burner in the uniform magnetic field
Fig. 3.11(a)	Refractive index difference of partially premixed flame of butane torch burner in the upward-decreasing magnetic field
Fig. 3.11(b)	Temperature distribution of partially premixed flame of butane torch burner in the upward-decreasing magnetic field
Fig. 3.12(a)	Refractive index difference of partially premixed flame of butane torch burner in the upward-increasing magnetic field
Fig. 3.12(b)	Temperature distribution of partially premixed flame of butane torch burner in the upward-increasing magnetic field
Fig. 3.13(a)	Photograph and recorded interferogram of premixed flame of butane torch burner in absence of magnetic field
Fig. 3.13(b)	Photograph and recorded interferogram of premixed flame of butane torch burner in uniform magnetic field.
Fig. 3.13(c)	Photograph and recorded interferogram of premixed flame of butane torch burner in upward-decreasing magnetic field
Fig. 3.13(d)	Photograph and recorded interferogram of premixed flame of butane torch burner in upward-increasing magnetic field
Fig. 3.14(a)	Refractive index difference of premixed flame of butane torch burner in the absence of magnetic field

Fig. 3.14(b)	Temperature distribution of premixed flame of butane torch burner in the absence of magnetic field
Fig. 3.15(a)	Refractive index difference of premixed flame of butane torch burner in the uniform magnetic field
Fig. 3.15(b)	Temperature distribution of premixed flame of butane torch burner in the uniform magnetic field
Fig. 3.16(a)	Refractive index difference of premixed flame of butane torch burner in the upward-decreasing magnetic field
Fig. 3.16(b)	Temperature distribution of premixed flame of butane torch burner in the upward-decreasing magnetic field
Fig. 3.17(a)	Refractive index difference of premixed flame of butane torch burner in the upward-increasing magnetic field
Fig. 3.17(b)	Temperature distribution of premixed flame of butane torch burner in the upward-increasing magnetic field
Fig. 3.18	Radial distribution of mole fraction of oxygen
Fig 4.1	Schematic of micro diffusion flame
Fig. 4.2(a)	Photograph of micro-flame created by mixture of C_2H_4 and air
Fig. 4.2(b)	Schematic of micro-flame created by mixture of C_2H_4 and air
Fig. 4.3	Photograph of the micro-diffusion candle flame
Fig. 4.4	Cross section of axi-symmetric temperature field
Fig. 4.5	Schematic of experimental set-up of circular grating Talbot interferometer for the measurement of temperature of micro-diffusion flame

Fig. 4.6	Photograph of experimental set-up of circular grating Talbot interferometer for the measurement of temperature of micro-diffusion flame
Fig. 4.7(a)	Recorded Interferogram of micro-diffusion flame in absence of magnetic field
Fig. 4.7(b)	Recorded Interferogram of micro-diffusion flame in uniform magnetic field
Fig. 4.7(c)	Recorded Interferogram of micro-diffusion flame in upward-decreasing magnetic field
Fig. 4.7(d)	Recorded Interferogram of micro-diffusion flame in upward-increasing magnetic field
Fig. 4.8	Flow chart of calculation
Fig. 4.9(a)	Filtered interferogram in the absence of magnetic field
Fig. 4.9(b)	Wrapped phase of recorded interferogram in the absence of magnetic field
Fig. 4.10(a)	Three-dimensional unwrapped phase along line AB in the absence of magnetic field
Fig. 4.10(b)	Two-dimensional unwrapped phase along line AB in the absence of magnetic field
Fig. 4.11(a)	Refractive index distribution along line AB in the absence of magnetic field
Fig. 4.11(b)	Temperature distribution profile along line AB in the absence of magnetic field
Fig. 4.12(a)	Temperature distribution profile along line AB in uniform magnetic field
Fig. 4.12(b)	Temperature distribution profile along line AB in upward-decreasing magnetic field
Fig. 4.12(c)	Temperature distribution profile along line AB in upward-increasing magnetic field

Fig. 5.1	Schematic of off axis digital holographic set-up for recording a hologram
Fig. 5.2	Process for the reconstruction of digital hologram
Fig. 5.3:	Schematic of Co-ordinate system used for recording and reconstruction of digital hologram
Fig. 5.4	Schematic of axi-symmetric temperature field of micro flame
Fig. 5.5(a)	Schematic of experimental set-up for the measurement of temperature distribution of wick stabilized micro diffusion flame created from candle
Fig. 5.5(b)	Photograph of experimental set-up for the measurement of temperature distribution of wick stabilized micro diffusion flame created from candle
Fig. 5.6	Schematic of various combinations of magnetic field and wrapped phase difference maps of air in absence and presence of micro flame under the three different configuration of magnetic field
Fig. 5.7(a)	Wrapped phase difference map of micro flame in the absence of uniform magnetic field
Fig. 5.7(b)	2D unwrapped phase difference map of micro flame corresponding to Fig (a) in the absence of uniform magnetic field
Fig. 5.7(c)	3D unwrapped phase difference map in the absence of uniform magnetic field
Fig. 5.7(d)	Unwrapped phase difference profile along line AB as marked in Fig. 5(a), in the absence of uniform magnetic field
Fig. 5.7(e)	Refractive index difference profile along line AB in the absence of uniform magnetic field
Fig. 5.7(f)	Temperature profile along line AB in the absence of uniform magnetic field

Fig. 5.8(a)	Wrapped phase difference maps of micro flame in the presence of uniform magnetic field
Fig. 5.8(b)	Temperature profile along the line AB in the presence of uniform magnetic field
Fig. 5.9(a)	Wrapped phase difference map of micro flame in the absence of magnetic field
Fig. 5.9(b)	Wrapped phase difference map of micro flame in the presence of upward decreasing magnetic field
Fig. 5.9(c)	Temperature profile along line AB corresponding to fig 5.9(a) in the absence of magnetic field
Fig. 5.9(d)	Temperature profile along line AB corresponding to fig 5.9(b) in the presence of upward decreasing magnetic field
Fig. 5.10(a)	Wrapped phase difference map of micro flame in the absence of magnetic field
Fig. 5.10(b)	Wrapped phase difference map of micro flame in the presence of upward increasing magnetic field
Fig. 5.10(c)	Temperature profile along line AB in the absence of magnetic field
Fig. 5.10(d)	Temperature profile along line AB in the presence of upward increasing magnetic field
Fig. 5.11(a)	Reconstructed wrapped phase difference of micro flame and ambient air for the 12 recorded holograms at the interval of 1 minute
Fig. 5.11(b)	Temperature profile for the 12 recorded holograms of micro flame along line AB corresponding to wrapped phase difference maps as shown in Fig 5.11(a)
Fig. 5.11(c)	Variation in maximum temperature (K) of micro flame at Point A versus time (Minutes) corresponding to temperature profile as shown in Fig 5.11(b)

Fig. 5.12(a)	Photograph of normal diffusion flame
Fig. 5.12(b)	Wrapped phase difference map of normal diffusion flame
Fig. 5.12(c)	Temperature profile of normal diffusion flame along line AB as marked on Fig. 5.12(b)
Fig. 5.12(d)	Photograph of micro diffusion flame
Fig. 5.12(e)	Wrapped phase difference map of micro diffusion flame
Fig. 5.12(f)	Temperature profile of micro flame along line AB as marked on Fig. 5.12(e)
Fig. 6.1(a)	Schematic of experimental set-up for onion epidermis cell imaging
Fig. 6.1(b)	Photograph of experimental set-up for onion epidermis cell imaging
Fig. 6.2(a)	Recorded image of USAF resolution test chart
Fig. 6.2(b)	Reconstructed intensity image of USAF resolution test chart
Fig. 6.2(c)	Line profile along line AB of USAF resolution test chart
Fig. 6.3(a)	Onion epidermis cell imaging slide preparation
Fig. 6.3(b)	Recorded image of onion epidermis cell
Fig. 6.4	Flow chart of phase calculation
Fig. 6.5(a)	Two-dimensional amplitude image of onion epidermis cell
Fig. 6.5(b)	Three-dimensional amplitude image of onion epidermis cell

Fig. 6.6	Three-dimensional phase profile of onion epidermis cell
Fig. 6.7(a)	Schematic of experimental set-up for red blood cell imaging
Fig. 6.7(b)	Photograph of experimental set-up for red blood cell imaging
Fig. 6.8(a)	Recorded image of USAF resolution test chart
Fig. 6.8(b)	Reconstructed wrapped phase image of USAF resolution test chart
Fig. 6.8(c)	Line profile along line AB of USAF resolution test chart on unwrapped phase image
Fig. 6.9(a)	Recorded image of polystyrene beads
Fig. 6.9(b)	3D Unwrapped phase of polystyrene beads
Fig. 6.10(a)	3D thickness map of polystyrene bead
Fig. 6.10(b)	Thickness profile along line AB of polystyrene bead
Fig. 6.11	3D unwrapped phase map and calculated thickness profile corresponding to selected beads
Fig. 6.12(a)	Recorded image of RBC
Fig. 6.12(b)	2D wrapped phase of RBC
Fig. 6.12(c)	3D unwrapped phase of RBC
Fig. 6.13(a)	2D unwrapped phase of selected portion of RBC
Fig. 6.13(b)	3D unwrapped phase of selected portion of RBC

Fig. 6.14(a)	3D unwrapped phase of single RBC
Fig. 6.14(b)	Unwrapped phase profile along line AB
Fig. 6.15	3D unwrapped phase map and obtained diameter of RBC
Fig. 6.16(a)	3D thickness map of RBC
Fig. 6.16(b)	Thickness profile of RBC

LIST OF TABLES

Table 2.1	Summary of the data extracted from the analysis of Talbot interferometric fringe pattern for different displacement values
Table 3.1	Butane diffusion flame parameter in magnetic field
Table 4.1	Dimension of created candle flame used for experiments
Table 4.2	Micro-diffusion flame flow characteristic in magnetic field
Table 5.1	Width of micro flame under three different configurations of magnetic fields

LIST OF SYMBOLS

a	Grating pitch
λ	Wavelength of the laser light
Z_T	Talbot distance
K	Integer
p/q	Fractional integer
ΔZ	Distance of fractional Talbot image
G1	First grating
G2	Second grating
(x, y, z)	Cartesian co-ordinate
$u_{1Before}$	Amplitude distribution (Field) before first grating
k	Propagation vector
i	Imaginary unit ($\sqrt{-1}$)
g_1	Transmittance of grating G1
m	Grating G1 order
C_m	Fourier expansion coefficient of m order grating
$u_0(x, y)$	Two dimensional object transmittance function

u_{1After}	Amplitude distribution (Field) after first grating
z_1	Distance between grating G1 and object plane
$u_{2Before}$	Amplitude distribution (Field) before second grating
g_2	Transmittance of grating G2
n	Grating G2 order
C_n	Fourier expansion coefficient of n order grating
z_2	Distance between grating G2 and object plane
u_{2after}	Amplitude distribution (Field) after second grating
M	Constant
C	Constant phase distribution of wavefront representation
I	Intensity distribution
u_{2After}^*	Complex conjugate of amplitude distribution (Field) after second grating
R	Distance between grating G1 and point source
r, φ	Polar co-ordinates of grating G1 plane
r	Radial location of any point on the grating
$2A$	Diameter of the circular grating
g_r	Fourier exponential series expression for grating transmittance

ϕ	Phase
D	Distance between grating G1 and G2
r', ϕ'	Polar co-ordinates of grating G2 plane
J_0	Zero order Bessel function
ϵ_x	Difference between grating G1 and G2 center
N	Constant coefficient under Dirac Delta function
Δx	Displacement value
x_f	Final position of point
x_i	Initial position of point
l	Integer (for the value of number of ring from grating center)
l'	Integer (for the value of number of ring from grating center)
$(1+\alpha)$	Change in pitch along the y-axis after deflection
$(1+\beta)$	Change in pitch along the z-axis after deflection
m'	Fringe number
ψ	Angle of deflection
Z_k	Distance between the object (burner) and second grating
n_m	Refractive index of medium

T_0	Temperature at the reference condition
n_0	Refractive index at the reference condition (air)
P_{atm}	Atmospheric pressure
A_m	Molar refractivity of air at 632.8 nm
R_g	Universal gas constant
F	Magnetic force
χ	Susceptibility of the chemical species
H	Magnetic field strength
a_h	Height of the micro flame
W_f	Width of micro flame
t_l	Characteristic time of travel from the burner exit to the bottom of the flame
d	Diameter of the burner tube
u_e	Fuel exit velocity at the burner port
u_d	Characteristic molecular diffusion velocity
l_D	Characteristic diffusion length
D_w	Diameter of wick
L_f	Length of Flame

L_b	Overlapping length of wick and flame
HT	Hilbert transform
$u(x)$	Real function
$z(x)$	Complex analytic signal
$l(x, z)$	Path length travelled by the light beam inside the axisymmetric temperature field
$\Delta n(r)$	Change in refractive index inside the flame
R_1	Maximum radial distance inside the flame
Q_f	Volumetric flow rate of fuel (m^3/sec)
T_m	Maximum flame temperature
S	Molar stoichiometric air-fuel ratio
X_{O_2}	Mole fraction of oxygen in air
m_f	Total fuel mass flow rate
C_p	Specific heat of gas at constant pressure
K	Thermal conductivity
s	Mass oxygen to fuel stoichiometric ratio
T_{vap}	Vaporization/boiling point of wax
N_a	Avogadro number

g_l	Lande's g-factor
μ_b	Bohr magneton
k	Boltzmann constant
S_i	Total electron spin
m_i	Molecular weight of species i
f_{max}	Maximum spatial frequency
Q	Fringe spacing
θ_{max}	Maximum angle between the object and reference wave
X_O	X -coordinate in object plane
Y_O	Y -coordinate in object plane
X_H	X -coordinate in hologram plane
Y_H	Y -coordinate in hologram plane
X_I	X -coordinate in image plane
Y_I	Y -coordinate in image plane
$O(X, Y)$	Object wave
$R(X, Y)$	Reference wave
$H(X, Y)$	Intensity distribution at hologram plane

$L \times B$	CCD rectangular aperture dimension containing
$M \times N$	Number of pixels on CCD sensor
ΔX_H	Sampling interval along X axis in the hologram plane
ΔY_H	Sampling interval along Y axis in the hologram plane
ρ	Distance between a point in the hologram plane and a point in the image plane
ΔX_I	Sampling interval along X axis in the image plane
ΔY_I	Sampling interval along Y axis in the image plane
$R(p, q)$	Digitized reference wave
$H(p, q)$	Digitized recorded intensity
$\Delta X_I, \Delta Y_I$	Pixel sizes in the reconstructed image
[S]	Area matrix
a_p	Interval between the measured pixel
$\Delta\phi$	Phase difference
B	Magnetic induction (Tesla)
μ_0	Magnetic permeability of free space (Henry/meter)
κ_a	Volumetric susceptibility of air

κ_f	Volumetric susceptibility of flame
κ_w	Volumetric susceptibility of molten wax near the wick
P_{af}	Pressure at interface of surrounding air and flame
P_{fw}	Pressure at the interface of flame and molten wax
$A(x)$	Background intensity distribution
B	Constant
P	Cauchy principal integral
n_p	Refractive index of polystyrene bead